Effects of passive components on the input current interharmonics of adjustable-speed drives

Soltani, Hamid; Blaabjerg, Frede; Zare, Firuz; Loh, Poh Chiang

Published in:
I E E E Journal of Emerging and Selected Topics in Power Electronics

DOI (link to publication from Publisher):
10.1109/JESTPE.2015.2505306

Publication date:
2016

Document Version
Accepted author manuscript, peer reviewed version

Effects of Passive Components on the Input Current Interharmonics of Adjustable-Speed Drives

Hamid Soltani, *Student Member, IEEE,* Frede Blaabjerg, *Fellow, IEEE,* Firuz Zare, *Senior Member, IEEE,* and Poh Chiang Loh, *Senior Member, IEEE*

***Abstract*—Current and voltage source Adjustable Speed Drives (ASDs) exert distortion current into the grid, which may produce some interharmonic components other than the characteristic harmonic components. This paper studies the effects of passive components on the input current interharmonics of adjustable speed drives with and/or without motor current imbalance. The investigation is done at different motor operating frequencies and load torque values. It shows that selecting the small filter components (AC choke, DC choke and DC-link capacitor) results in different performances in respect to those interharmincs issued by motor current imbalance and other non-characteristic interharmonics. The results are helpful for engineers investigating the effects of drive filters on the input current interharmonic components.**

***Index Terms*—Adjustable speed drive, passive component effects, interharmonics, harmonics, balanced and unbalanced load.**

I. Introduction

INTERHARMONICS are spectral components of voltages or currents which are not multiple integer of the fundamental supply frequency [1]. Although interharmonics extents are usually smaller than those of characteristic harmonics, their still increasing effects on the power supply have recently drawn more concerns and there are on-going global discussions to define some limits for these components. Severe voltage flicker, interference with control and protection signals in power supply lines, overheating of transformers, dormant resonance excitation are among some of the most common direct effects of interharmonics [2]–[4]. Double-stage variable speed drives either voltage source or current source are presently among the main sources of interharmonics injected into the power supplies in addition to typical harmonics [5]–[11], where a variable speed motor is fed through an AC/DC/AC converter with normally a diode-bridge rectifier and a PWM inverter connected back-to-back sharing a common DC link.

If the DC link is not well buffered by a sufficiently large capacitor or inductor, the inverter output current frequency components will pass through the DC link and the rectifier and will then interact with the input current frequency components, consequently give rise to unsteady current distortions. In this regard, increasing the DC-link capacitor or the inductor may be an attractive solution, but it has its own limitations such as higher cost and volume and maybe also a shorter compromised lifetime of the converters. In addition, the advanced achievements in the design of the capacitors with longer lifetime and more voltage fluctuation tolerance made them promising to be used in power converter applications.

Till now, several investigations have been initiated focusing more on the interharmonics sources and their negative effects on the power supply [12]–[17]. In [18], the interharmonics generation process is addressed in high power ASD based on double-stage conversion systems implementing line commutated or pulse width modulated inverters. In [19], an analytical method has been proposed for the assessment of the harmonic and interharmonic currents initiated by ASD under unbalanced supply conditions. Moreover, the effect of motor current imbalance on the input current interharmonics in the voltage source inverter fed ASD has been comprehensively discussed in [20]. The authors in [21], [22] proposed some active compensation methods to reduce the ASD input current interharmonics caused by motor current imbalance. In addition to the above-mentioned studies, some other investigations are initiated for accurate identification of interharmonic components. Encountering with the fact that small errors in synchronizing the time window and ten cycles of the estimated system fundamental frequency may cause significant spectral leakage phenomenon, the authors in [23] have suggested the utilization of the Hanning window instead of the Rectangular window recommended by IEC [24]. The authors in [25] have also proposed a self-tuning algorithm to synchronize the analyzed window width to an integer multiple of the actual fundamental frequency prior to interharmonic evaluation. In [26], a frequency-domain interpolation approach has been used to find the system fundamental frequency, and the interpolatory polynomial method has been implemented for reconstructing the sampled time-domain signal.Then by applying the FFT and the frequency-domain interpolation, the actual harmonic and interharmonic components have been calculated respectively.

Besides many investigations done related to the interharmonic sources and identifications, with a global movements toward using smaller passive filters (AC choke, DC choke and DC-link capacitor) for ASD, it is needed to consider the effects of these passive components on the interharmonic issues. Although, the authors in [14] discussed the relative effects of DC-link inductance and source inductance on interharmonic propagation, there is still a special need to consider the direct effects of the filter components on the input current interharmonics at different working points of ASD. This paper first investigates the disturbance (initiated by motor

H. Soltani, F. Blaabjerg and P. C. Loh are with the Department of Energy Technology, Aalborg University, Aalborg 9220, Denmark (e-mail: hso@et.aau.dk; fbl@et.aau.dk; pcl@et.aau.dk).

F. Zare is with Danfoss Drives A/S, Global Research & Development Centre Ulsnaes 1, DK-6300 Graasten, Denmark (e-mail: fza@danfoss.com).

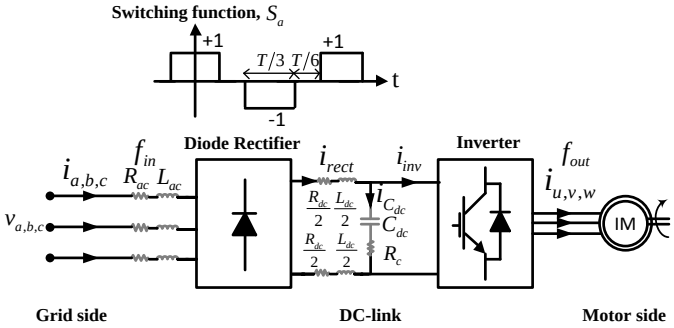

Fig. 1. Equivalent circuit of an adjustable-speed drive for system analysis with an Induction Motor (IM).

unbalanced currents) propagation from the inverter output side to the rectifier input side of the ASD. Then, the effects of ASD passive filter components on the grid-side current interharmonics will be analyzed in five different cases, while the motor currents are unbalanced. Finally, the filter effects on the input current total interharmonic distortions, in the case of the balanced load, at different motor operating frequencies and load torque values are investigated.

II. Unbalanced Load Conditions

A. Interharmonics initiated by load current imbalance

Fig. 1 shows a schematic diagram of the VSI-fed adjustable speed drive for analyzing the input current interharmonic components. The Space Vector Modulation (SVM) method is chosen for the modulation because of its superior performance characteristics especially in adjustable speed drive applications. In this case, the existence of a current distortion at the inverter output gives rise to the grid side current interharmonics. Scaling and offset errors in the adjustable speed drives current transducers, unbalanced loads and also overmodulation operating mode of the inverters are typically the main sources of the inverter output current imbalance. The following analysis explains how the inverter current distortions may lead to input current interharmonic components.

In accordance with the symmetrical component theory, the three-phase unbalanced motor currents $\{i_u, i_v, i_w\}$ can be separated into three sets of balanced and uncoupled components: the positive-sequence current components ($\{i_u^p, i_v^p, i_w^p\}$ with magnitude I_{out}^p frequency w_{out} and phase θ_{out}^p) and the negative-sequence components ($\{i_u^n, i_v^n, i_w^n\}$ with magnitude I_{out}^n frequency w_{out} and phase θ_{out}^n),which can be written as (1)

$$\begin{cases} i_u = i_u^p + i_u^n = I_{out}^p sin\left(\omega_{out}t + \theta_{out}^p\right) \\ \quad\quad +I_{out}^n sin\left(\omega_{out}t + \theta_{out}^n\right) \\ i_v = i_v^p + i_v^n = I_{out}^p sin\left(\omega_{out}t + \theta_{out}^p - \frac{2\pi}{3}\right) \\ \quad\quad +I_{out}^n sin\left(\omega_{out}t + \theta_{out}^n + \frac{2\pi}{3}\right) \\ i_w = i_w^p + i_w^n = I_{out}^p sin\left(\omega_{out}t + \theta_{out}^p + \frac{2\pi}{3}\right) \\ \quad\quad +I_{out}^n sin\left(\omega_{out}t + \theta_{out}^n - \frac{2\pi}{3}\right) \end{cases} \quad (1)$$

The inverter-side DC-bus average current can be obtained by the sum of the DC-link inverter-side current i_{inv} over one output fundamental period. Fig. 2 shows the three-phase output

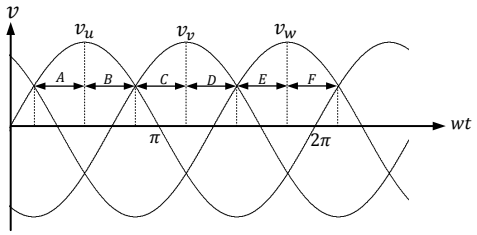

Fig. 2. Three-phase output reference signals.

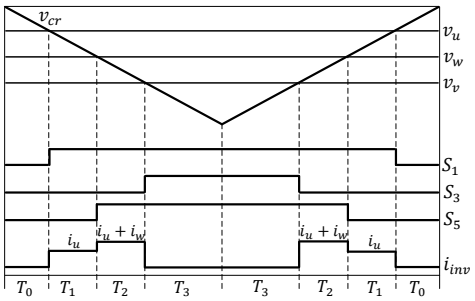

Fig. 3. PWM and DC-link inverter-side current waveforms in interval A.

reference signals $\{v_u, v_v, v_w\}$ and the related six intervals used in space vector modulation. The PWM signals and the corresponding DC-link inverter-side current over one switching period T_s in interval A are also illustrated in Fig. 3, where S_1, S_3 and S_5 are the gating signals of the inverter upper switches associated with the three-phase output reference signals v_u, v_v and v_w respectively. Based on this figure and the three-phase unbalanced motor currents in (1), the average DC-link current $I_{inv,A}$ over one switching period in interval A can simply be obtained as

$$\begin{cases} I_{inv,A} = \frac{1}{T_s}\int_0^{T_s} i_{inv}\,dt = \frac{2T_1}{T_s}i_u + \frac{2T_2}{T_s}(i_u + i_w) \\ = \frac{3}{4}mI_{out}^p cos\left(\theta_{out}^p\right) - \frac{3}{4}mI_{out}^n cos\left(2\omega_{out}t + \theta_{out}^n\right) \end{cases} \quad (2)$$

where m is the modulation index and T_1 and T_2 are time durations specified in Fig. 3 and they can be calculated as

$$\begin{cases} T_1 = \frac{mT_s}{4}(sin(w_{out}t) - sin(w_{out}t + \frac{2\pi}{3})) \\ T_2 = \frac{mT_s}{4}(sin(w_{out}t + \frac{2\pi}{3}) - sin(w_{out}t - \frac{2\pi}{3})) \end{cases} \quad (3)$$

with the same calculations, the inverter-side DC-bus average current in all other five intervals will be similar as in (2), which finally results in the DC-link inverter-side average current I_{inv} for one fundamental cycle of the inverter output current

$$\begin{cases} I_{inv} = I_{dc} + I_{\sim inv} cos\left(2w_{out}t + \theta_{inv}\right) \\ = \frac{3}{4}mI_{out}^p cos\left(\theta_{out}^p\right) - \frac{3}{4}mI_{out}^n cos\left(2\omega_{out}t + \theta_{out}^n\right) \end{cases} \quad (4)$$

where I_{dc} and $I_{\sim inv}$ are the desired DC current and the oscillation components of the inverter-side DC-bus current respectively. From (4) it can be seen that the output current unbalance causes a harmonic component, which is twice the output frequency in addition to the DC quantity. The DC component in (4) is associated with the fundamental positive-sequence current and the AC component is related to the presence of the motor current imbalance. According to the circuit law, the inverter-side DC-bus current is divided as $i_{inv} = i_{rect} - i_{Cdc}$, where i_{rect} and i_{Cdc} are the DC currents

TABLE I
SIMULATION PARAMETER VALUES FOR STUDY OF INTERHARMONICS IN ASD.

Parameter	Case 1	Case 2	Case 3	Case 4	Case 5
Rated Input Power	2.2 kW	2.2 kW	2.2 kW	2.2 kW	2.2 kW
Rated Input Voltage	400 V	400 V	400 V	400 V	400 V
Inverter Carrier Frequency	5 kHz	5 kHz	5 kHz	5 kHz	5 kHz
DC-link Capacitor & Resistor, C_{dc}&R_c	125 μF & 500 mΩ	125 μF & 500 mΩ	125 μF & 500 mΩ	15 μF & 100 mΩ	15 μF & 100 mΩ
Inductor & Resistor, L_{dc} & R_{dc}	$--$	8 mH & 360 mΩ	2 mH & 90 mΩ	$--$	900 μH & 40 mΩ
Input Inductor & Resistor, L_{ac}&R_{ac}	6 mH & 270 mΩ	$--$	4.5 mH & 200 mΩ	900 μH & 40 mΩ	$--$
Motor Nominal Input Voltage	380 V	380 V	380 V	380 V	380 V

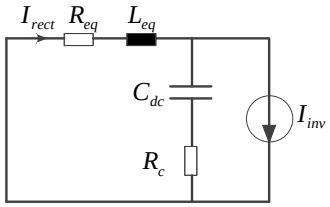

Fig. 4. DC-link equivalent circuit for motor drive harmonic analysis.

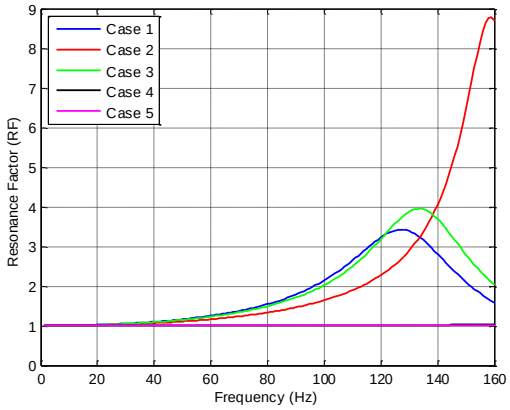

Fig. 5. DC-link resonance factor associated with Case 1 to Case 5.

flowing out of the rectifier DC terminals and through the DC-link capacitor. Therefore the rectifier-side DC-bus average current I_{rect} will have oscillation at twice the inverter output operating frequency and it can be expressed as (5)

$$I_{rect} = I_{dc} + I_{\sim rect} cos\left(2w_{out}t + \theta_{rect}\right) \tag{5}$$

The second term in (5) is a ripple component with magnitude, frequency and phase notated as $I_{\sim rect}$, $2w_{out}$ and θ_{rect}. The DC-link equivalent circuit depicted in Fig. 4 represents the current transfer from the inverter DC side to the rectifier DC side. Considering a Continuous Conduction Mode (CCM) operation of the front-end diode rectifier, the equivalent DC-link inductance L_{eq} and damping resistance R_{eq} are [20]

$$L_{eq} = L_{dc} + 2L_{ac} \tag{6}$$

$$R_{eq} = R_{dc} + 2(R_{ac} + r_d) + \frac{3}{\pi} w_{in} L_{ac} \tag{7}$$

where the last term in (7) accounts for the voltage drop caused by diode commutations, w_{in} is the grid voltage angular frequency and r_d denotes the diode dynamic resistance. In order to assess the effects of passive components on the DC-link disturbance current excitations, five different cases (Case 1 to Case 5) whose parameter values are listed in Table I are taken into account in this study. The DC-link resonance factors RF, defined in (8), are drawn in Fig. 5.

$$RF = \frac{I_{\sim rect}}{I_{\sim inv}} = \frac{Z_C}{Z_C + Z_L} \tag{8}$$

Based on Fig. 5, from one point of view, there is almost no DC-link resonance excitation associated with the last two cases in which the drive filter components (AC choke, DC choke and DC-link capacitor) values are much smaller than those of the first three cases, within the motor frequency range (0 to 50 Hz). Obviously, the higher resonance frequencies (about 970 Hz and 1370 Hz for Case 4 and Case 5 respectively) associated with the last two cases may excite the dormant current oscillations located at those regions. In another point of view, adopting the larger values for the filter components may not necessarily lead to lower current oscillations transferring from the inverter DC side to the rectifier DC side. Actually, by selecting the larger DC-link filters, the corresponding DC-link resonance frequency will decrease and consequently it may even worsen the current oscillations located at lower frequencies. Thus depending on the motor operating condition, the drive filter design needs specific attention concerning the DC-link disturbance excitations.

After leaking through the DC-link stage, the second order oscillation of the DC-link rectifier-side current will be multiplied by the rectifier switching functions $\{S_a, S_b, S_c\}$. Using Fourier series analysis, the rectifier switching function S_a observed in Fig. 1 can be obtained as given in (9). Thereafter, the rectifier switching functions in (9), when multiplied with the rectifier-side DC-bus current presented at (5), gives rise to the three-phase input current expressions as given in (10). From (10), it is evident that the distortion currents initiated by the

$$\begin{cases} S_a(t) = 2\sqrt{3}/\pi \left[\cos(w_{in}t) - 1/5\cos\left(5w_{in}t\right) + 1/7\cos\left(7w_{in}t\right) - 1/11cos(11w_{in}t) + \ldots\right] \\ S_b(t) = S_a\left(t - T/3\right) \\ S_c(t) = S_a\left(t + T/3\right) \end{cases} \tag{9}$$

$$\begin{cases} i_a(t) = S_a I_{rect} = \left(2\sqrt{3}I_{dc}/\pi\right)\left[\cos(w_{in}t) - 1/5\cos\left(5w_{in}t\right) + 1/7\cos\left(7w_{in}t\right) + \ldots\right] \\ \quad + \left(\sqrt{3}I_{\sim rect}/\pi\right)\left\{\left[\cos((w_{in}+2w_{out})\,t + \theta_{rect}) + \cos((w_{in}-2w_{out})\,t - \theta_{rect})\right]\right. \\ \quad -1/5\left[\cos((5w_{in}+2w_{out})\,t + \theta_{rect}) + \cos((5w_{in}-2w_{out})\,t - \theta_{rect})\right] \\ \quad \left.+1/7\left[\cos((7w_{in}+2w_{out})\,t + \theta_{rect}) + \cos((7w_{in}-2w_{out})\,t - \theta_{rect})\right] + \ldots\right\} \\ i_b(t) = i_a\left(t - T/3\right) \\ i_c(t) = i_a\left(t + T/3\right) \end{cases} \tag{10}$$

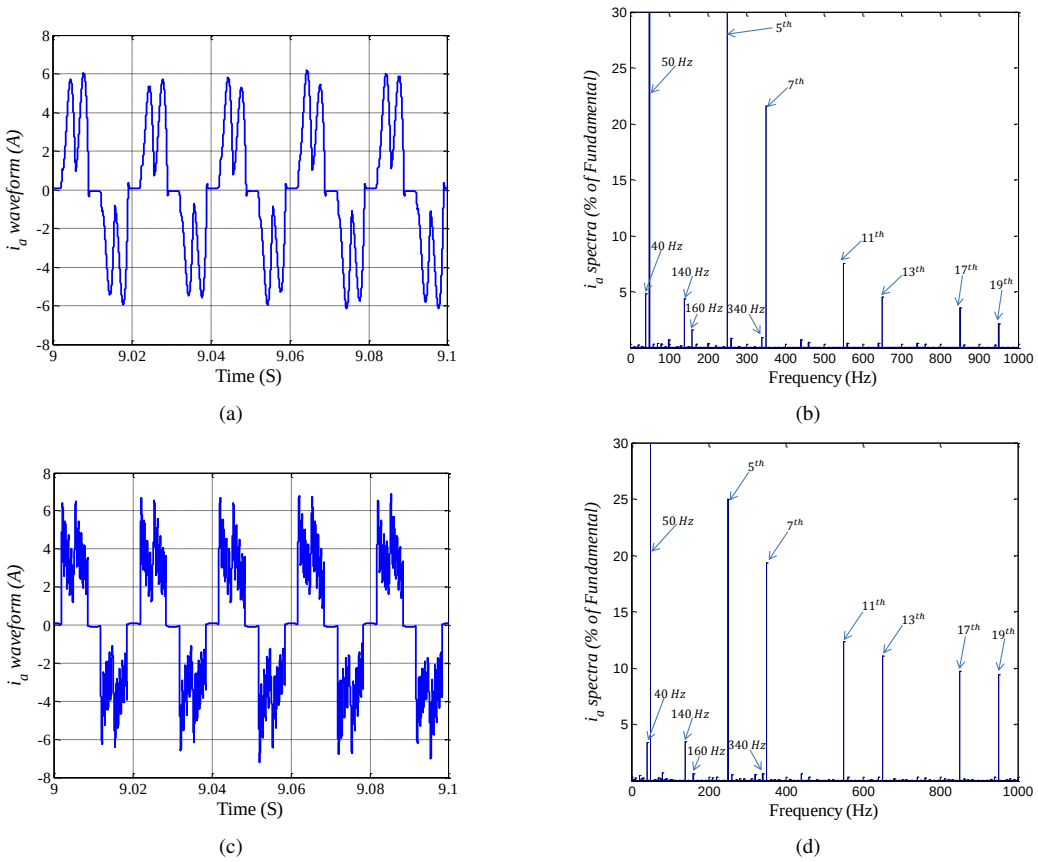

Fig. 6. Drive input current i_a waveforms and frequency spectrum at load torque TL value of 12 Nm, and an output frequency f_{out} of 45 Hz with cases from Table I. (a) Input current waveform in Case 1. (b) Input current spectra in Case 1. (c) Input current waveform in Case 5. (d) Input current spectra in Case 5.

motor current imbalance pass through the double-stage ASD and then generate interharmonic currents in the power system. These exclusive interharmonic components are accommodated symmetrically around the input side fundamental frequency and the characteristic harmonics. According to (10), although higher order interharmonics may have much lower magnitudes, they are potentially able to excite parallel resonances in the grid. Fig. 6 depicts the drive input current waveforms with the corresponding frequency spectra at the load torque T_L value of 12 Nm and the output frequency f_{out} of 45 Hz for Case 1 and Case 5 respectively. As it can be seen from Figs. 6(b) and (d), the input current contains interharmonic components located at the frequencies of $|90 \pm 50|$ Hz, $|90 \pm 250|$ Hz, $|90 \pm 350|$ Hz, and etc. However, some interharmonic components, other than those generated by the motor current imbalance, can also be recognized in the input current spectra, Figs. 6(b) and (d).

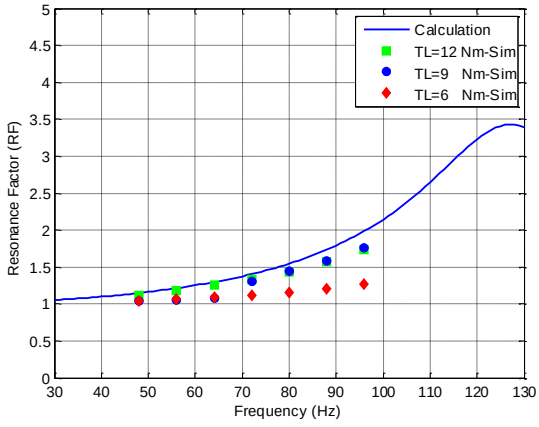

Fig. 7. DC-link resonance factor associated with Case 1 (see Table I) at different output frequencies and load torque values.

B. Effect of passive components

In this section, the effects of adjustable speed drive filters (as defined in Table I) on the input current interharmonic components are studied. A series of simulations have been carried out in MATLAB using the simulation model shown in Fig. 1. A 2.2 kW induction motor is considered with the output frequency range of f_{out}=24 Hz to 48 Hz, at three different constant load torque values of T_L=12 Nm, 9 Nm and 6 Nm. The motor is controlled by using a simple constant voltage-to-frequency method and an inductor of 4 mH was also added to emulate the motor-winding imbalance. As a consequence, a motor current imbalance of about five to six percent was provided at different output speeds at each constant load torque value.

Fig. 7 illustrates the DC-link resonance factor associated with Case 1, at different output frequencies and load torque values. As it can be observed, less current disturbance amplifications occur at the DC link for the lower load torque value of 6 Nm in which the front-end diode rectifier operates almost in Discontinuous Conduction Mode (DCM). It can also be noted that the calculation results (blue solid line) and simulations (green square points) have a good agreement at the load torque value of 12 Nm, where the front-end diode rectifier works in CCM mode. The same convergence can also be viewed for the load torque value of 9 Nm (blue dots), above the DC-link oscillation frequency of 70 Hz.

In accordance with (10), the grid current interharmonic components initiated by the motor current imbalance mainly appear around the fundamental frequency and its harmonics. Nonetheless, only those interhamonics around the grid current fundamental and fifth order frequencies, which normally have larger amplitudes are plotted in Fig. 8. It should be noted that all interharmonic values, I_i, illustrated in Fig. 8, Fig. 10, and Fig. 11 are calculated in accordance with (11)

$$I_i = \frac{I_{ipeak}}{I_{fpeak}} \tag{11}$$

where I_{ipeak} and I_{fpeak} are the peak values of the related grid current interharmonic and the fundamental frequency respectively. The index i also represents the related interharmonic frequency.

At a constant load torque, the input current interharmonic components will increase when the motor output speed increases, especially for the first sets of interharmonics around the fundamental frequency, as seen in Fig. 8. Based on Fig. 8, it is also obvious that the DC-link resonance factors, as already shown in Fig. 7, are in good harmony with those interharmonic components accommodated around the supply current fundamental frequency ($I_{f_{in}-2f_{out}}$ and $I_{f_{in}+2f_{out}}$ depicted in Fig. 8(a) and Fig. 8(b) respectively). However, the interharmonics located around the fifth order harmonic ($I_{5f_{in}-2f_{out}}$ and $I_{5f_{in}+2f_{out}}$ shown in Fig. 8(c) and Fig. 8(d)) may not follow the associated DC-link current disturbance amplifications. It is worth to mention that for the interharmonic

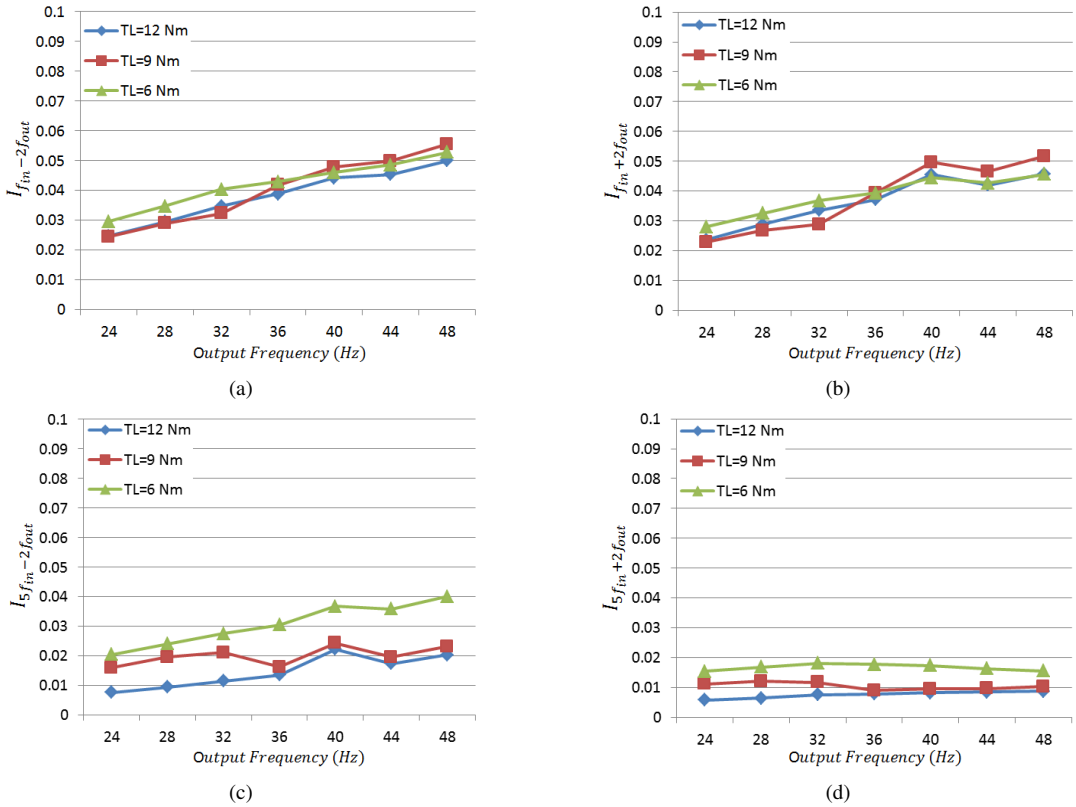

Fig. 8. Normalized input current interharmonic components in Case 1 (see Table I) versus output frequencies of the ASD at different load torque values. (a) Interharmonics coupled with and below the fundamental frequency $I_{f_{in}-2f_{out}}$. (b) Interharmonics coupled with and above the fundamental frequency $I_{f_{in}+2f_{out}}$. (c) Interharmonics coupled with and below the fifth order frequency $I_{5f_{in}-2f_{out}}$. (d) Interharmonics coupled with and above the fifth order frequency $I_{5f_{in}+2f_{out}}$.

components surrounding the fifth order harmonic, the lower load torque values are almost associated with the higher relative interharmonic entities, Fig. 8(c) and Fig. 8(d).

Fig. 9 compares the DC-link resonance factor values related to Case 1 to Case 5 at the output frequency range of 24 Hz to 48 Hz in three constant load torque values (equal to 12 Nm, 9 Nm and 6 Nm). As expected, the last two cases (Case 4 and Case 5) show lower DC-link current disturbance amplification from the inverter DC side to the rectifier DC side. Moreover, considering the equal output current imbalance and modulation index for the first three cases, the Case 2 shows less harmonic amplification in the DC link, at the load torque value of 12 Nm (which is close to the full load operating mode of ASD), Fig. 9(a). However, Fig. 9(c) depicts that for the load torque of 6 Nm (which is close to the half load operating mode of ASD), the Case 2 is associated with a higher DC-link resonance factor.

A comprehensive comparison of the input current interharmonics related to the the five investigated cases at the output frequency range of 24 Hz to 48 Hz and the load torques of 12 Nm and 6 Nm are plotted in Fig. 10 and Fig. 11. Based on Fig. 10(a) and Fig. 10(b), among the first three cases, the Case 2 represents smaller interharmonic values at the lower motor output speeds (below 36 Hz) for those interharmonics accommodated around the grid current fundamental frequency. This is while for the higher output speed ranges, these interharmonics take higher values in the Case 2. At the load torque equal to 12 Nm, it can also be seen that the last two investigated cases show almost better performance in all operating conditions, as shown in Fig. 10. At lower load torque value of 6 Nm, the Case 2 is steadily corresponded with the higher values of the input current interharmonic components, Fig. 11. In addition, the superior performance of the last two cases in respect to the current interharmonic components located around the fifth order grid current frequency are observed in Fig. 11(c) and Fig. 11(d).

The results presented so far clearly show that with the presence of any possible output current imbalance, a suitable design of the equivalent DC-link filters may lead to a better performance of the ASD handling the input current interharmonics. It also shows that Case 2 (i.e. putting the filters in the DC side of the front end diode rectifier) is usually related to higher values of the interharmonics, especially when the motor is operating near the nominal speed at full load torque operating mode and/or it functions at the low load torque conditions.

Following the global trends toward implementing smaller DC-link filter components in ASD applications, the last two cases were devoted to analyze their effects on the ASD input current interharmonics. The results demonstrate the superior performances of the last two cases compared with the first three cases in terms of input current interharmonics caused by motor unbalanced currents. However, considering very high resonance frequencies related to the last two cases, it is needed to study their performances at the higher disturbance frequencies of the DC-link current.

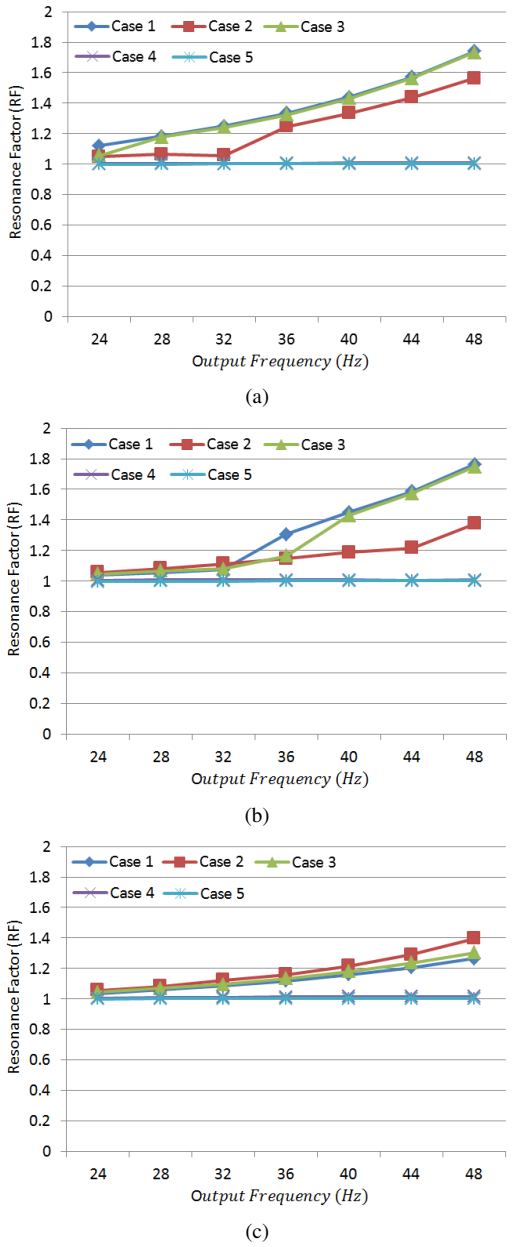

Fig. 9. DC-link resonance factors associated with Case 1 to Case 5 versus different output frequencies of the ASD. (a) load torque equal to 12 Nm. (b) load torque equal to 9 Nm. (c) load torque equal to 6 Nm.

III. Balanced Load Conditions

In this section the possible effects of the equivalent DC-link passive filters on the input current interharmonics are studied considering a balanced operating mode for ASD. Like the unbalanced load condition, the investigated parameters are used as given in Table I. In order to assess the drive input current quality in the five above-mentioned cases, three of the indices are taken into account:

- the Total Harmonic current Distortion (THD)
- the Total Interharmonic current Distortion up to 2 kHz (TIHD_{2kHz})
- the total interharmonic current distortions between 2 kHz to 9 kHz (TIHD_{2-9kHz})

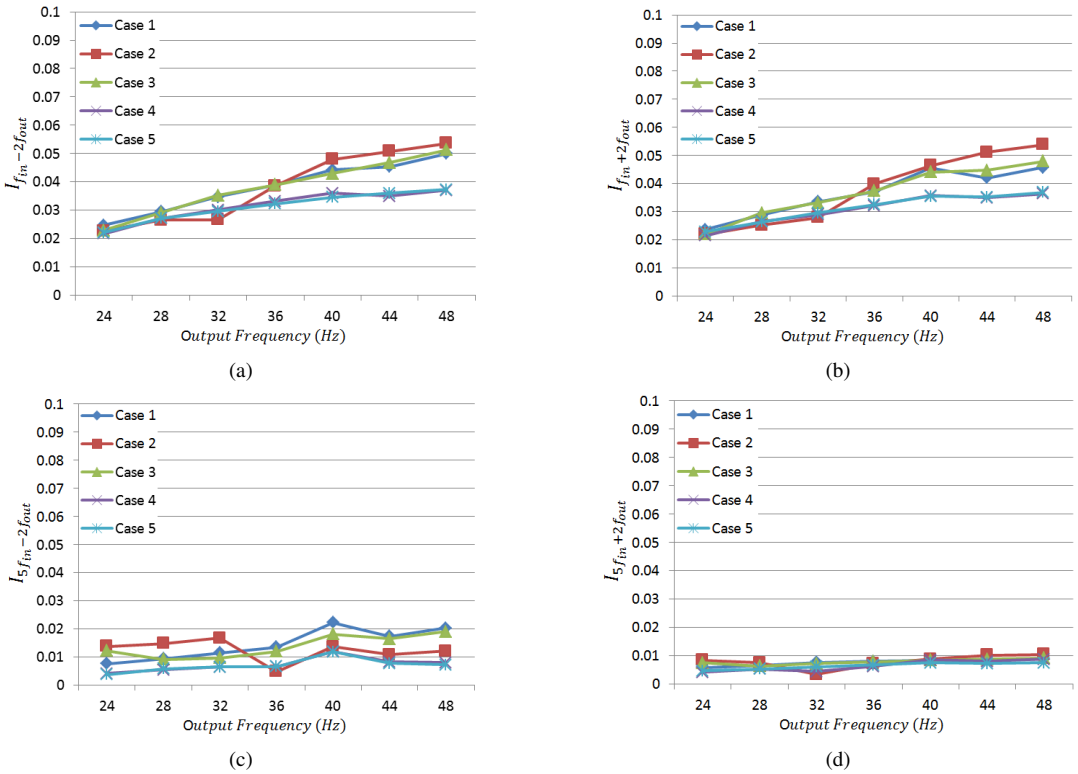

Fig. 10. Normalized input current interharmonic components in Case 1 to Case 5 versus output frequencies of the ASD at the load torque equal to 12 Nm. (a) Interharmonics coupled with and below the fundamental frequency $I_{f_{in}-2f_{out}}$. (b) Interharmonics coupled with and above the fundamental frequency $I_{f_{in}+2f_{out}}$. (c) Interharmonics coupled with and below the fifth order frequency $I_{5f_{in}-2f_{out}}$. (d) Interharmonics coupled with and above the fifth order frequency $I_{5f_{in}+2f_{out}}$.

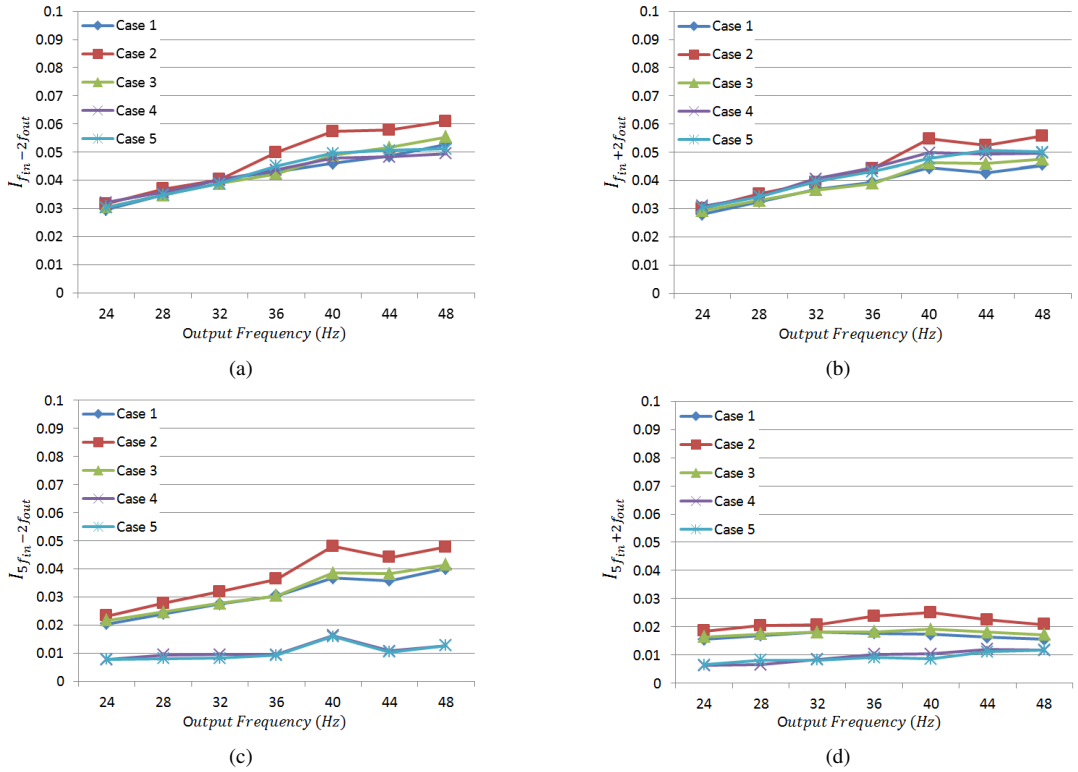

Fig. 11. Normalized input current interharmonic components in Case 1 to Case 5 versus output frequencies of the ASD at the load torque equal to 6 Nm. (a) Interharmonics coupled with and below the fundamental frequency $I_{f_{in}-2f_{out}}$. (b) Interharmonics coupled with and above the fundamental frequency $I_{f_{in}+2f_{out}}$. (c) Interharmonics coupled with and below the fifth order frequency $I_{5f_{in}-2f_{out}}$. (d) Interharmonics coupled with and above the fifth order frequency $I_{5f_{in}+2f_{out}}$.

These indices are considered as (12)-(14)

$$THD = \frac{\sqrt{\sum_{h \in H} I_h^2}}{I_1}, \ H = \text{set of harmonics} \tag{12}$$

$$TIHD_{2kHz} = \frac{\sqrt{\sum_{ih \in \Lambda} I_{ih}^2}}{I_1}, \ \Lambda = \text{set of interharmonics up to 2 kHz} \tag{13}$$

$$TIHD_{2-9\,kHz} = \frac{\sqrt{\sum_{ih \in \gamma} I_{ih}^2}}{I_1}, \ \gamma = \text{set of interharmonics between 2 to 9 kHz} \tag{14}$$

The importance of the defined indices can be considered for the compatibility problem and the tough regulations for interharmonic components. In the case of linear modulation and balanced loading, the input current interharmonics in ASD usually accommodate around the switching frequency and its integer multiple components other than those appearing at the lower frequencies. This was the reason of choosing two different indices ($TIHD_{2kHz}$ and $TIHD_{2-9kHz}$) for interharmonic assessment. It should also be noted that the obtained results are based on 1-Hz resolution spectral analysis.

The input current total harmonic distortion THD traces at the motor output frequency range of 24 Hz to 48 Hz and three load torque values of 12 Nm, 9 Nm and 6 Nm are plotted in Fig. 12. It can be observed that the results associated with Case 5 demonstrate its significant performances specially at high load torque values, even though it benefits from small filter components. From this standpoint and with taking the input current THD values into consideration, choosing small components as ASD filters will make them even competitive compared with selecting larger filters for ASD. Moreover, between the first three investigated cases (Case 1 to Case 3), the traces show the priority of the Case 1 at different operating modes. Fig. 13 illustrates the input current total interharmonic distortions ($TIHD_{2kHz}$ and $TIHD_{2-9kHz}$) of the ASD in the Case 1 to Case 5 at two load torque values of 12 Nm and 6 Nm. Unlike the promising results of Case 5 in respect to the THD values especially at higher load torque condition, as shown in Fig. 12, this case represents the worst condition regarding interharmonic components. This phenomenon is more evident at the total current interharmonic distortions between 2 kHz to 9 kHz, Fig. 13(b) and Fig. 13(d), where $TIHD_{2-9kHz}$ increases significantly at the higher output frequencies of the motor. With comparing the results related to the load torque values of 12 Nm and 6 Nm, it can also be seen that the lower torque value gives higher current interharmonic distortions. Meanwhile, among the first three investigated cases, the Case 2 presents the worst condition in respect to interharmonic distortions. Moreover, due to the fact that the DC-link resonances in the first three cases are accommodated at low frequencies, their effects on interharmonic magnification are less than the last two cases in which the DC-link resonances are located at higher frequencies (during balanced operating mode of ASD, the interharmonics components usually appear at higher frequencies). With the on-going interests towards using a small DC-link filters for ASD, the depicted results here necessitate to consider interharmonic distortions specially for those interharmonics accommodated above 2 kHz.

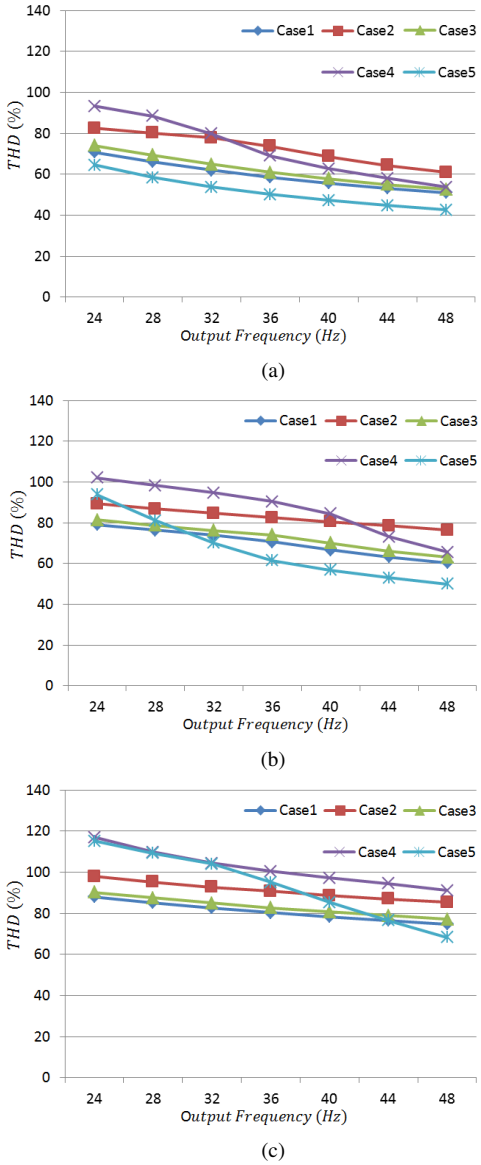

Fig. 12. ASD input current THD values associated with Case 1 to Case 5 (see Table I) at different output frequencies. (a) load torque equal to 12 Nm. (b) load torque equal to 9 Nm. (c) load torque equal to 6 Nm.

IV. Conclusion

In this paper, the effects of ASD passive filters on the grid current interharmonics are investigated at separate drive output frequencies and also different load torque values. Particular attention is given to both cases of the unbalanced and balanced operating modes of ASD. The results show that in discontinuous conduction mode of the front-end diode rectifier, the DC-link resonance amplification decreases, however it does not necessarily mean a lower input current interharmonic distortion.

In the unbalanced operating condition, using small filter components for ASD results in a competitive performance

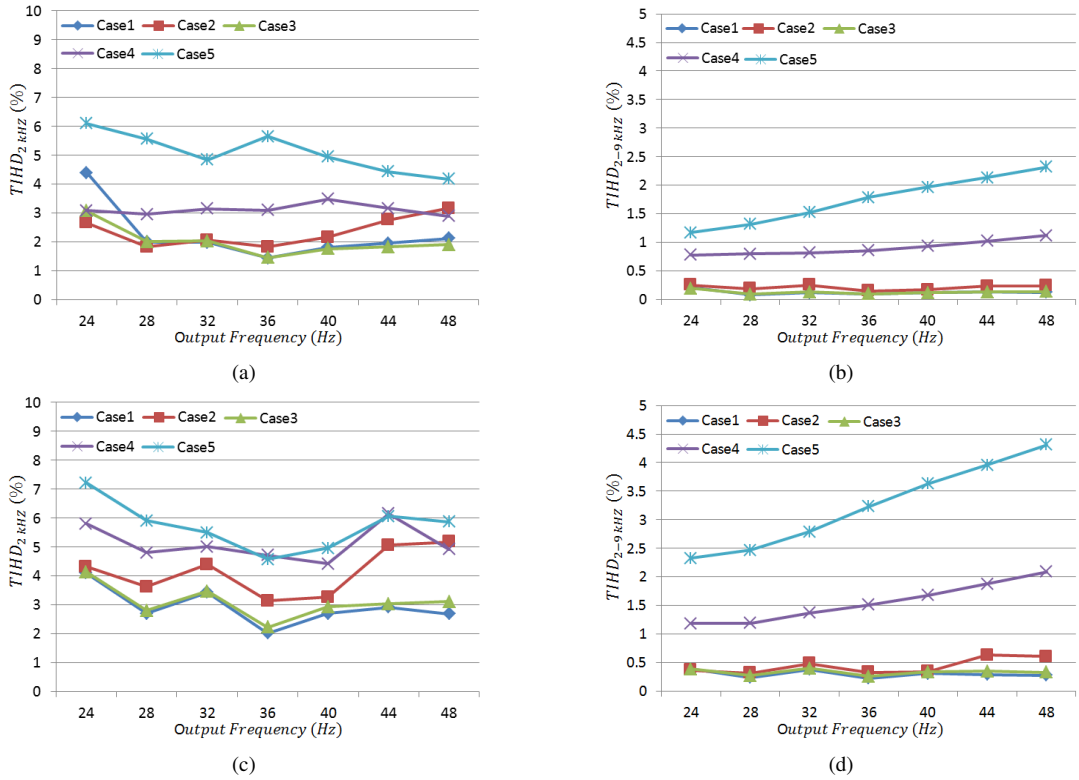

Fig. 13. Input current total interharmonic distortions in Case 1 to Case 5 (see Table I) versus output frequencies of the ASD. (a) TIHD_{2kHz} at the load torque of 12 Nm. (b) TIHD_{2-9kHz} at the load torque of 12 Nm. (c) TIHD_{2kHz} at the load torque of 6 Nm. (d) TIHD_{2-9kHz} at the load torque of 6 Nm.

in comparison with the larger filter components. However, for the balanced operating mode the results depicted a weak performance for the smaller filters in respect to interharmonic distortions. Moreover, almost in all operating conditions (at the same operating speed), it is shown that the drive input current distortions are higher at the lower load torque values. The comparative results of the five investigated filter cases should be useful for engineers concerning the drive input current distortions at low and high frequency ranges.

REFERENCES

[1] A. Testa, M. Akram, R. Burch, G. Carpinelli, G. Chang, V. Dinavahi, C. Hatziadoniu, W. Grady, E. Gunther, M. Halpin *et al.*, "Interharmonics: theory and modeling," *IEEE Trans. Power Del.*, vol. 22, no. 4, pp. 2335–2348, Oct. 2007.

[2] D. Gallo, C. Landi, R. Langella, and A. Testa, "IEC flickermeter response to interharmonic pollution," presented at the 11th Int. Conf. Harmonics and Quality of Power, Lake Placid, NY, 2004, pp. 489–494.

[3] V. Wagner, J. Balda, D. Griffith, A. McEachern, T. Barnes, D. Hartmann, D. Phileggi, A. Emannuel, W. Horton, W. Reid *et al.*, "Effects of harmonics on equipment," *IEEE Trans. Power Del.*, vol. 8, no. 2, pp. 672–680, Apr. 1993.

[4] D. Gallo, R. Langella, A. Testa, and A. Emanuel, "On the effects of voltage subharmonics on power transformers: a preliminary study," presented at the 11th ICHQP, Lake Placid, NY, 2004, pp. 501–506.

[5] S. Hansen, L. Asiminoaei, and F. Blaabjerg, "Simple and advanced methods for calculating six-pulse diode rectifier line-side harmonics," in *Conf. Rec. IEEE 38th IAS Annu. Meeting*, 2003, pp. 2056–2062.

[6] M. Grötzbach, T. Strasser, and L. Lorenz, "Line Side Harmonics of Threephase Current Controlled Rectifiers in Continuous and Discontinuous Operation Mode," in *Proc. of IEEE-EPE Conf.*, 1993, pp. 707–712.

[7] D. E. Rice, "A detailed analysis of six-pulse converter harmonic currents," *IEEE Trans. Ind. Appl.*, vol. 30, no. 2, pp. 294–304, Mar./Apr. 1994.

[8] Y. Baghzouz, "An accurate solution to line harmonic distortion produced by AC/DC converters with overlap and DC ripple," *IEEE Trans. Ind. Appl.*, vol. 29, no. 3, pp. 536–540, May/Jun. 1993.

[9] M. Grötzbach, M. Bauta, and R. Redmann, "Line side behavior of six-pulse diode bridge rectifiers with AC-side reactance and capacitive load," in *Proc. of Power Quality Conf.*, 1995, pp. 525–534.

[10] L. Asiminoaei, F. Blaabjerg, and S. Hansen, "Harmonic calculation toolbox in industry application for adjustable speed drive," in *Proc. of IEEE-APEC Conf.*, vol. 3, 2004, pp. 1628–1634.

[11] P. Davari, Y. Yang, F. Zare, and F. Blaabjerg, "A multi-pulse pattern modulation scheme for harmonic mitigation in three-phase multi-motor drives," *IEEE J. Emerg. Sel. Top. Power Electron.*, vol. PP, no. 99, pp. 1–12, Jul. 2015.

[12] R. Yacamini, "Power system harmonics. Part 4: Interharmonics," *Power Eng. J.*, vol. 10, no. 4, pp. 185–193, Aug. 1996.

[13] W. Xu, H. W. Dommel, M. B. Hughes, G. W. Chang, and L. Tan, "Modelling of adjustable speed drives for power system harmonic analysis," *IEEE Trans. Power Del.*, vol. 14, no. 2, pp. 595–601, Apr. 1999.

[14] M. Rifai, T. H. Ortmeyer, and W. J. McQuillan, "Evaluation of current interharmonics from ac drives," *IEEE Trans. Power Del.*, vol. 15, no. 3, pp. 1094–1098, Jul. 2000.

[15] R. Carbone, F. De Rosa, R. Langella, and A. Testa, "A new approach for the computation of harmonics and interharmonics produced by line-commutated AC/DC/AC converters," *IEEE Trans. Power Del.*, vol. 20, no. 3, pp. 2227–2234, Jul. 2005.

[16] G. W. Chang and S. K. Chen, "An analytical approach for characterizing harmonic and interharmonic currents generated by VSI-fed adjustable speed drives," *IEEE Trans. Power Del.*, vol. 20, no. 4, pp. 2585–2593, 2005.

[17] L. Feola, R. Langella, and A. Testa, "On the effects of unbalances, harmonics and interharmonics on PLL systems," *IEEE Trans. Instrum. Meas.*, vol. 62, no. 9, pp. 2399–2409, Sep. 2013.

[18] F. De Rosa, R. Langella, A. Sollazzo, and A. Testa, "On the interharmonic components generated by adjustable speed drives," *IEEE Trans. Power Del.*, vol. 20, no. 4, pp. 2535–2543, Oct. 2005.

[19] G. W. Chang, S. K. Chen, H. J. Su, and P. K. Wang, "Accurate assessment of harmonic and interharmonic currents generated by VSI-

fed drives under unbalanced supply voltages," *IEEE Trans. Power Del.*, vol. 26, no. 2, pp. 1083–1091, Apr. 2011.
[20] D. Basic, "Input current interharmonics of variable-speed drives due to motor current imbalance," *IEEE Trans. Power Del.*, vol. 25, no. 4, pp. 2797–2806, Oct. 2010.
[21] H. Soltani, P. C. Loh, F. Blaabjerg, and F. Zare, "Interharmonic analysis and mitigation in adjustable speed drives," in *Conf. Rec. IECON 40th Annu. Meeting*, 2014, pp. 1556–1561.
[22] H. Soltani, P. Loh, F. Blaabjerg, and F. Zare, "Interharmonic mitigation of adjustable speed drives using an active DC-link capacitor," in *Proc. ICPE-ECCE Asia*, 2015, pp. 2018–2024.
[23] A. Testa, D. Gallo, and R. Langella, "On the processing of harmonics and interharmonics: using Hanning window in standard framework," *IEEE Trans. Power Del.*, vol. 19, no. 1, pp. 28–34, Jan. 2004.
[24] *Power Quality Measurement Methods, Testing and Measurement Techniques*, IEC Std. 61000-4-30.
[25] D. Gallo, R. Langella, and A. Testa, "A self-tuning harmonic and interharmonic processing technique," *Eur. Trans. Elect. Power*, vol. 12, no. 1, pp. 25–31, Jan./Feb. 2002.
[26] G. Chang, C. Chen, Y. Liu, and M. Wu, "Measuring power system harmonics and interharmonics by an improved fast Fourier transform-based algorithm," *IET Gener., Transm., Distrib.*, vol. 2, no. 2, pp. 193–201, Mar. 2008.

Hamid Soltani (S'14) received B.Sc. and M.Sc. degrees in electrical engineering from the University of Mazandaran (Noushirvani), Babol, Iran, in 2005 and 2008, respectively. From 2009 to 2013, he was with the Department of Electrical and Computer Engineering, Golestan University, Gorgan, Iran, as a lecturer. He is currently working toward the Ph.D. degree from the Department of Energy Technology, Aalborg University, Aalborg, Denmark. His current research interests include harmonics analysis, power quality, power electronics topologies and control.

Frede Blaabjerg (S'86–M'88–SM'97–F'03) was with ABB-Scandia, Randers, Denmark, from 1987 to 1988. From 1988 to 1992, he was a Ph.D. Student with Aalborg University, Aalborg, Denmark. He became an Assistant Professor in 1992, an Associate Professor in 1996, and a Full Professor of power electronics and drives in 1998. His current research interests include power electronics and its applications such as in wind turbines, PV systems, reliability, harmonics and adjustable speed drives. He has received 15 IEEE Prize Paper Awards, the IEEE PELS Distinguished Service Award in 2009, the EPE-PEMC Council Award in 2010, the IEEE William E. Newell Power Electronics Award 2014 and the Villum Kann Rasmussen Research Award 2014. He was an Editor-in-Chief of the IEEE TRANSACTIONS ON POWER ELECTRONICS from 2006 to 2012. He has been Distinguished Lecturer for the IEEE Power Electronics Society from 2005 to 2007 and for the IEEE Industry Applications Society from 2010 to 2011. He is nominated in 2014 by Thomson Reuters to be between the most 250 cited researchers in Engineering in the world.

Firuz Zare (S'98–M'01–SM'06) received his Ph.D. in Power Electronics from Queensland University of Technology in 2002. He has spent several years in industry as a team leader and development engineer working on power electronics and power quality projects. Dr. Zare won a student paper prize at the Australian Universities Power Engineering Conference (AUPEC) conference in 2001 and was awarded a Symposium Fellowship by the Australian Academy of Technological Science and Engineering in 2001. He received the Vice Chancellor's research award in 2009 and faculty excellence award in research as an early career academic from Queensland University of Technology in 2007. Dr. Zare has published over 150 journal and conference papers and technical reports in the area of power electronics. He is currently a Lead Engineer with Danfoss Power Electronics, Graasten, Denmark. He is a Task Force Leader of Active Infeed Converters within Working Group one at the IEC Standardization Committee. His current research interests include problem-based learning in power electronics, power electronics topologies and control, pulsewidth modulation techniques, EMC/EMI in power electronics, and renewable energy systems.

Poh Chiang Loh received the B.Eng. and M.Eng. degrees from the National University of Singapore, Singapore, in 1998 and 2000, respectively, and the Ph.D. degree from Monash University, Clayton, Vic., Australia, in 2002, all in electrical engineering. From 2003 to 2009, he was an Assistant Professor with the Nanyang Technological University, Singapore, and since 2009, he has been an Associate Professor in the same university. In 2005, he was a Visiting Staff first at the University of Hong Kong, and then at Aalborg University, Denmark. In 2007 and 2009, he again returned to Aalborg University first as a Visiting Staff involved in matrix converters and the inverters, and then as a Guest control of grid-interfaced Member of the Vestas Power Program. He is presently a Full Professor with Aalborg University, Aalborg, Denmark. His research interests are power electronics, power quality and microgrids.